

CHEMISTRY

Access to tetracyclic aromatics with bridgehead metals via metalla-click reactions

Zhengyu Lu^{1,2*}, Qin Zhu^{1*}, Yuanting Cai¹, Zhixin Chen¹, Kaiyue Zhuo¹, Jun Zhu¹, Hong Zhang^{1†}, Haiping Xia^{1,2†}

The never-ending pursuits for exploring aromatic molecular architectures result in the large libraries of aromatics with fascinating structures, which have greatly broadened the scope of aromaticity. Despite extensive efforts that have been paid to develop aromatic frameworks, the construction of polycyclic aromatics that share a bridgehead atom with more than three rings has never been accomplished. Here, an unprecedented family of aromatics, in which a metal center shared by 4 five-membered aromatic rings, has been achieved by using the metalla-click reactions with excellent yields and remarkable regioselectivity. The distinctive tetracyclic aromatics exhibit a broad absorption in the ultraviolet-visible near-infrared region and excellent thermal stability in air, enabling their potential applications in photoelectric materials and biomedicine. This study now makes it possible to incorporate four aromatic rings with one common sharing metal center by a straightforward strategy that would promote further development of previously unknown polycyclic complex motifs in aromatic chemistry.

INTRODUCTION

Molecular architectures with fascinating aromatic structures have attracted considerable interest across the scientific community, leading to the discovery of enormous aromatic molecules with structural variety. Among those aromatic frameworks, the fused-ring aromatic topology is intriguing as it features structural elegance and distinct properties (1–6). However, a bridgehead carbon atom can only secure up to three aromatic fused rings because of its inherent atomic orbital distribution. To realize creative fused-ring aromatic frameworks, heteroatoms have been incorporated into the aromatic rings (7–12). Transition metal atoms have also been designed as heteroatoms to formally replace at least one carbon unit of the archetypal aromatic hydrocarbons, affording a distinctive class of heterocycles, metalla-aromatics, through synergistic interplay of theoretical and experimental investigations. The participation of the *d*-atomic orbitals of the transition metal facilitates the construction of fused-ring aromatic frameworks, as exemplified by a number of two- or three-fused-ring metalla-aromatics having one bridgehead atom in common (13–20). Although theoretically feasible, the integration of more than three π -aromatic fused rings sharing one bridgehead atom remains elusive, even in transition metal-involving systems. We speculated that tricyclic metalla-aromatics with high reactivity could be used as excellent building blocks that, upon cycloaddition with unsaturated substrates, would lead to unprecedented polycyclic aromatic motifs. With this hypothesis, a tricyclic complex bearing an $M\equiv C$ bond was properly designed as starting material to explore straightforward annulation strategy via metalla-click reactions, i.e., the first [3 + 2] cycloadditions of a late transition metal carbyne with azides (Fig. 1). This strategy provides a convenient collection of extraordinary metal-bridgehead tetracyclic aromatics with a high degree of skeletal complexity and functional

diversity. Furthermore, these complexes, as new members of the aromatics family, exhibit remarkably broad absorption from the ultraviolet (UV) to the near-infrared (NIR) region, leading to excellent photothermic properties.

RESULTS AND DISCUSSION

Synthesis of tetracyclic aromatics via click reaction of cyclic metal carbyne complexes

As a classic click reaction, copper-catalyzed azide/alkyne cycloaddition (CuAAC) features the formation of a five-membered aromatic heterocycle, i.e., 1,2,3-triazole, with high reaction efficiency under mild reaction conditions (21, 22). In recent years, Houk and co-workers reported that the high reactivity of strain-promoted Huisgen cycloadditions (in the absence of copper catalysts) is due to the lower energy required to distort the 1,3-dipole and alkyne into the transition-state geometry (23, 24). We thus envisaged that constraining transition metal carbynes into small rings would lead to the activation of the $M\equiv C$ bond and offer access to the 1,3-dipolar cycloadditions with azides. On the basis of our previous investigation of metallapentalynes (25–29), the synthesis of the activated $M\equiv C$ bond within the tricyclic ring system was then targeted, in the hope of obtaining suitable starting material to generate desired tetracyclic aromatic motifs through metalla-click reactions. We reacted complex **1** (27) with K_2CO_3 (5 eq) at 40°C for 2 days, which afforded a green solution, from which complex **2** was isolated in 84% yield (Fig. 2A). Complex **2** was characterized by nuclear magnetic resonance (NMR) spectroscopy and high-resolution mass spectrometry (HRMS). In the ^{13}C NMR spectrum, the signal for the carbyne carbon of complex **2** was observed at 337.2 parts per million (ppm), which is close to the reported value for osmapentalynes (25–28). The solid-state structure of complex **2** was further confirmed by single-crystal x-ray diffraction via counter anion exchange of Cl with BPh_4 (Fig. 2B; see the Supplementary Materials for details). The x-ray diffraction study revealed that **2** has a fused metallapentalyne core structure with good planarity, as reflected by the small mean deviation (0.034 Å) from the least-squares plane through Os1, O1, and C1–C9. The bond distance of the Os1–C1 [1.888(5) Å] and the bond angle at the

¹State Key Laboratory of Physical Chemistry of Solid Surfaces, Collaborative Innovation Center of Chemistry for Energy Materials (iChem), College of Chemistry and Chemical Engineering, Xiamen University, Xiamen 361005, China. ²Department of Chemistry, Shenzhen Grubbs Institute, Southern University of Science and Technology, Shenzhen 518055, China.

*These authors contributed equally to this work.

†Corresponding author. Email: zh@xmu.edu.cn (H.Z.); hpxia@xmu.edu.cn (H.X.)

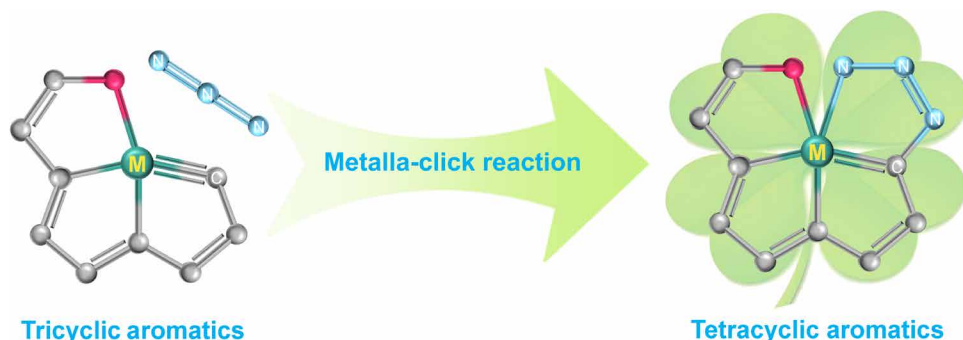


Fig. 1. Designed tricyclic source enables the access to tetracyclic aromatics with bridgehead metals by metalla-click reaction.

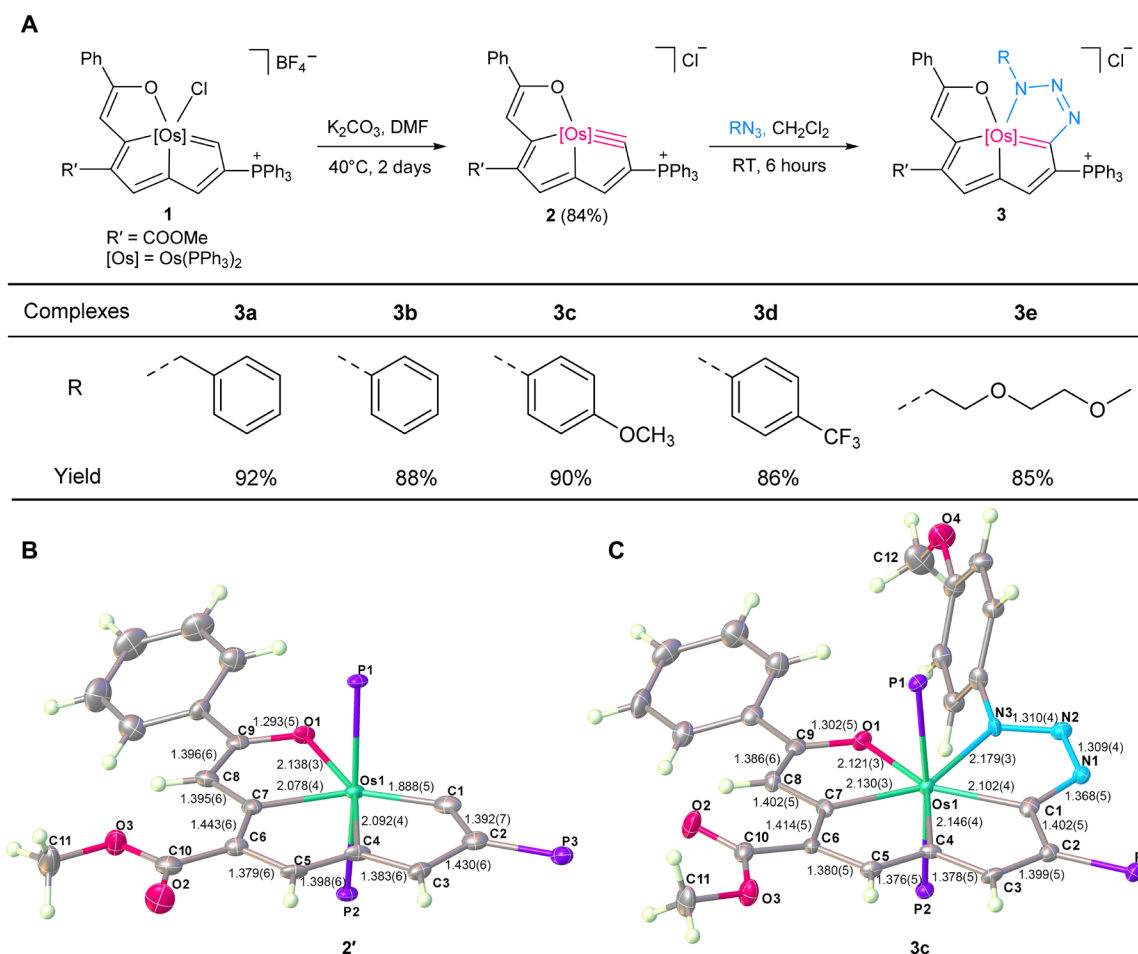


Fig. 2. Synthesis of polycyclic aromatics **2** and **3**. (A) Designed fused osmium complex containing an $\text{M}\equiv\text{C}$ bond enables metalla-click reactions with azides. (B) Molecular structure of the cation of **2'** (drawn with 50% probability). The phenyl moieties in PPh_3 are omitted for clarity. (C) Molecular structure of the cation of **3c** (drawn with 50% probability). The phenyl moieties in PPh_3 are omitted for clarity.

sp -hybridized carbon atom [$129.7(3)^\circ$] are comparable to those of previously reported metallapentalynes (25–29). The corresponding bond distances within the metallacycles, together with the planarity of the metallatrimethylene, indicate electronic delocalization within the metallatrimethylene in **2**. It is noted that **2** is the first cyclic metal carbyne in tricyclic metalla-aromatics with a bridgehead metal. This reaction achieves a rare transformation from a metallapentalene to a metallapentalyne (26, 30) and generates a late transition metal carbyne with

extremely high ring strain stemming from the small angle around $\text{C}_{\text{carbyne}}$ (129.7°) within the five-membered ring, thus motivating us to further examine the reactivity of **2** with azides.

As indicated by in situ NMR, stirring a mixture of **2** and benzyl azide in dichloromethane at room temperature for 6 hours resulted in almost quantitative conversion to complex **3a** (fig. S1), which was isolated in 92% yield. As illustrated in Fig. 2A, a series of azide substrates bearing different groups were also investigated. No intermediate

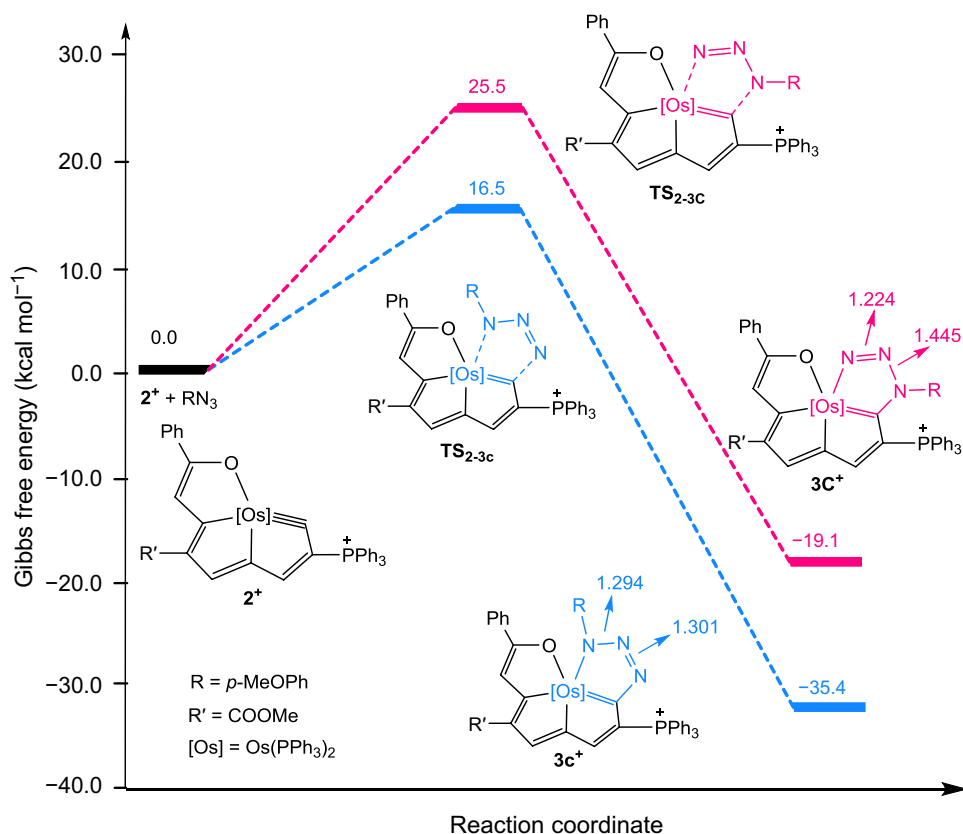
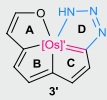
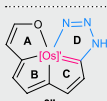
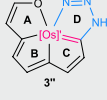
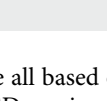


Fig. 3. Energy profiles for cycloaddition reactions of 4-anisyl azide and osmapentalene 2^+ calculated at the PCM-B3LYP-D3BJ/6-311++G(d,p)-LANL2TZ level. The Gibbs free energies and selected bond lengths are given in kilocalories per mole and angstroms, respectively. The pathway for the formation of the 4-substituted product ($3C^+$) is labeled in red, whereas that for the 2-substituted product ($3C^+$) is labeled in blue.

species were observed even when the reaction was carried out at low temperature (0°C), suggesting that the transformation of **2** and azides to **3** is quite facile. The results demonstrated good compatibility and efficiency of this reaction. A range of diversely functionalized azides readily participated in the reaction to afford the corresponding products **3b** to **3e** in 85 to 90% yields. These annulation products **3** exhibit good thermal stability both in solution and in the solid state. For example, the solid sample of **3a** can persist for several months when exposed to air at room temperature or even when heated at 100°C in air for 3 hours.

A single crystal of **3c** suitable for x-ray diffraction studies was obtained by recrystallization in hexane. The x-ray diffraction study established that the osmium-carbon bond is incorporated with the N_3 unit to form a planar, five-membered osmacycle (Fig. 2C). The most remarkable feature is the four-leaf clover motif, in which the osmium center arranges in a seven-coordinated pentagonal bipyramidal geometry and serves as a common vertex for 4 five-membered metallacycles (the bicyclic metallapentalene unit, the metallafuran unit, and the metallatriazole unit). The tetracyclic skeleton containing Os1, O1, C1–C9, and N1–N3 is approximately coplanar, as indicated by the mean deviation from the least-squares plane (0.114 \AA) and the sums of the angles of these four rings (540° , 539.7° , 540.0° , and 539.8° , which are close to the ideal value of 540°). All of the Os–C and C–C bond lengths in complex **3c** are similar to those reported for osmapentalene derivatives (27, 28, 30–35). The Os1–O1 (2.121 \AA) and C9–O1 (1.302 \AA) bond lengths are close to those reported for osmafurans (bond length ranges in this article

Table 1. NICS(1) values (in parts per million) of the 4 five-membered rings of the 2-substituted model **3'** and the 4-substituted model **3''** calculated at the B3LYP/6-311++G(d,p) level. [Os] = Os(PH₃)₂.

Model	NICS	A	B	C	D
	NICS(1)	-3.7	-10.9	-9.9	-7.3
	NICS(1) _{zz}	-5.4	-24.8	-21.3	-16.2
	NICS(1)	-3.2	-8.7	-8.7	-3.7
	NICS(1) _{zz}	-5.0	-18.0	-17.2	-4.8

are all based on a search from the Cambridge Structural Database, CSD version 5.39 in November 2017) and metallapentalenofurans (2.082 to 2.234 \AA for Os–O and 1.216 to 1.296 \AA for C–O, respectively) (27). Both the planarity and the delocalized bond lengths in **3c** suggest its delocalized structure. The planar metallatriazole unit in **3c** has more delocalized structural parameters than previously reported examples with early transition metal tungsten and molybdenum (36, 37). For instance, the N1–N2 (1.309 \AA), N2–N3 (1.310 \AA), and C1–N1 (1.368 \AA) bond lengths of **3c** fall within the range of N–N and C–N single and double bonds (bond length ranges in this article are all based on a search of the Cambridge Structural

Database, CSD version 5.39 in November 2017), respectively. Consistent with the solid structure, proton signals of the metallacycle were observed at 8.13 (H5), 8.02 (H8), and 7.62 (H3) ppm. In the ^{13}C NMR spectrum, the signals of metal-bonded C1 (233.9 ppm) and C7 (224.7 ppm) are shifted downfield compared with that of C4 (168.4 ppm), suggesting that C1 and C7 show more carbene character than C4.

Although the “alkyne-like” metal-carbon triple bond has been rarely used in click reactions, pioneering efforts in the 1990s established that molybdenum and tungsten carbynes can undergo cycloaddition reactions with azides, similar to the azide/alkyne cycloaddition, to form metallatriazole units (36, 37). The inherent nucleophilicity of the *sp* carbons in early transition metal carbynes might naturally facilitate the addition of azides. However, such reactions have remained largely unexplored for more than 20 years, as demonstrated by these two examples so far, and have never been achieved in the late transition metal carbyne species before.

Theoretical calculations

Note that only 2-substituted products were formed in the metallacyclic reactions of complex **2** with azides. To investigate the regioselectivity of this reaction, we calculated the B3LYP transition structures. As shown in Fig. 3, the Gibbs free energies of the transition states and products for the 2-substituted species (16.5 and -35.4 kcal/mol, respectively) were lower than those for the 4-substituted species (25.5 and -19.1 kcal/mol, respectively), suggesting that the 2-substituted product is both thermodynamically and kinetically favored. The bulky phosphonium substituent of **2** likely prevents the formation of the 4-substituted structure, exclusively yielding the sterically preferred 2-substituted product.

We found that the N–N bond lengths in the 2-substituted model compound **3c**⁺ (1.294 and 1.301 Å) are more average than those in the 4-substituted model **3c**⁺ (1.224 and 1.445 Å). The experimentally observed delocalized bond lengths, planarity of the tetracyclic

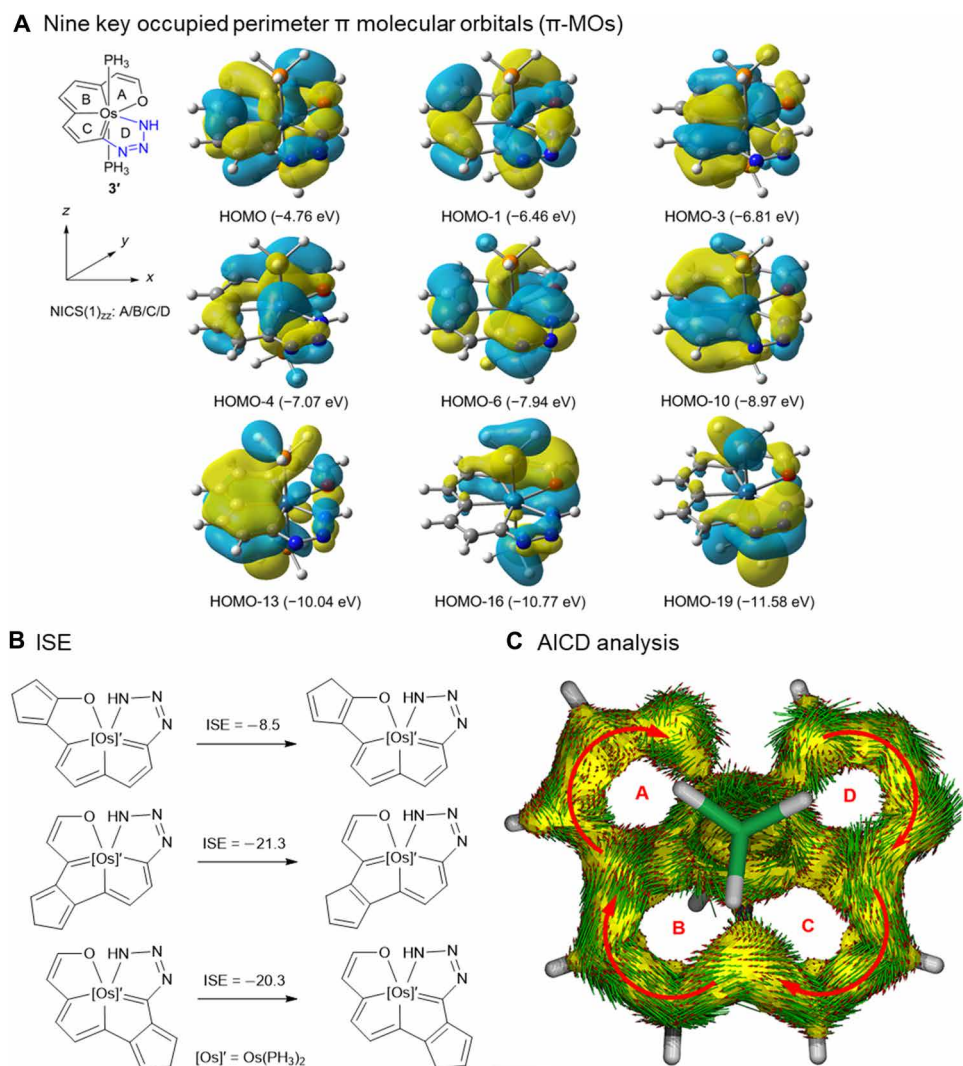


Fig. 4. Aromaticity evaluation. (A) Nine key occupied perimeter π molecular orbitals (π -MOs) of the model complex **3'**. The eigenvalues of the MOs are given in parentheses. (B) The aromaticity of model complex **3'** evaluated by the ISE method. The energies [in kilocalories per mole, computed with the B3LYP functional and the LanL2DZ basis set for Os and P and the 6 to 311++G(d,p) basis sets for C, O, N, and H] include zero-point energy corrections. (C) AICD plots of **3'** with the contribution from eight π -MOs. The molecular plane is placed perpendicular to the magnetic field vector. Isovalues for AICD isosurface is 0.025 arbitrary unit (a.u.). The diatropic ring currents indicate aromaticity.

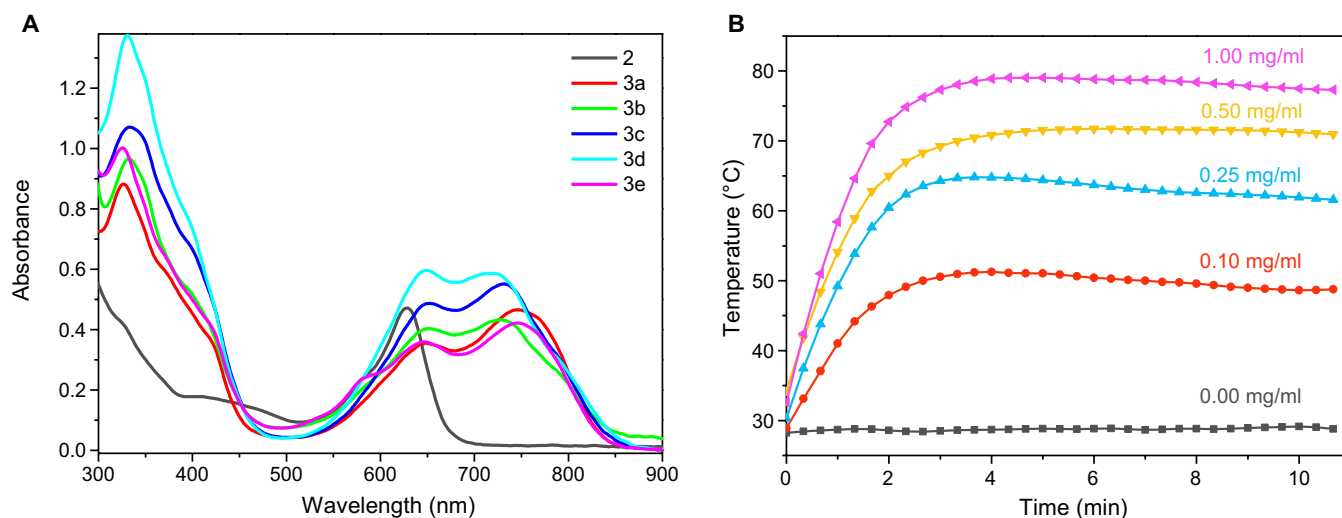


Fig. 5. UV-Vis-NIR absorption spectra and photothermal properties. (A) The absorption spectra of **2** and **3a** to **3e** (5.0×10^{-5} M) measured in dichloromethane solution at room temperature. (B) Temperature elevation of the solvent and solutions of complex **3a** at different concentrations (1.00, 0.50, 0.25, and 0.10 mg/ml) in 90% water-ethanol (*v/v*) solution upon laser irradiation (808 nm, 1 W/cm²).

framework, downfield chemical shifts of the metallacycle proton, and high stability indicate the aromaticity of **3**. Therefore, we calculated the nucleus-independent chemical shift (NICS) values (38) based on the unsubstituted model compounds **3'** and **3''** (the PPh₃ ligands were replaced by PH₃ groups). In general, negative NICS values indicate aromaticity, and positive NICS values indicate antiaromaticity. As shown in Table 1, the calculated NICS(1)_{zz} value for the metallatriazole unit (ring D) in **3'** is -16.2 ppm, whereas the value in **3''** is -4.8 ppm. The more negative NICS(1)_{zz} values, together with the more average of the bond lengths in the metallatriazole unit complex **3'**, indicate that the metallatriazole unit (ring D) in **3'** might be more stable than **3''** owing to the better aromaticity. We thus infer that the difference in aromaticity may also account for the high regioselectivity of the conversion from **2** to **3**. In addition, the NICS(1)_{zz} values of the other three fused metallacycles (rings A, B, and C) of **3'** are negative, whereas the values in the 4-substituted model **3''** are reduced to some extent. Therefore, the efficient cyclization reactions of late transition metal carbyne complex **2** with azides can be viewed as aromaticity-driven processes.

To elucidate the bonding and electronic structure of these unique tetracyclic aromatics, we performed density functional theory (DFT) calculations on simplified unsubstituted models of **3'**. The DFT-optimized structural parameters of **3'**, especially the bond distances in the metallacycles, agree well with those observed for the crystal structure of **3c**. The calculated Wiberg bond indices for Os1-C1, Os1-C4, Os1-C7, Os1-O1, and Os1-N3 in **3'** are 0.85, 0.75, 0.86, 0.54, and 0.67, respectively, indicating strongly covalent bonding between the metal center and the metal-bonded ring atoms. The main characteristic of the orbital interactions in metallacycles of **3'** is the involvement of two filled metal *d* orbitals of the metal center in the π bonding. The molecular orbitals (MOs) are derived principally from the orbital interactions between the *p π* orbitals of the organic fragment and the *d* orbitals of the Os atom ($5d_{xz}$ and $5d_{yz}$). The key occupied π -MOs (HOMO, HOMO-1, HOMO-3, HOMO-4, HOMO-6, HOMO-10, HOMO-13, HOMO-16, and HOMO-19) are identified as the valence π -MOs of the tetracyclic ring system

(Fig. 4A). However, as also demonstrated in previous examples (25), π orbitals that are not a “perimeter MO” may not contribute to the aromaticity of metallacycles. Because HOMO-3 has the most contribution from the Os d_{xz} orbital, which is not pointing along the perimeter of the ring, the tetracyclic system is considered as an aromatic molecule with planar 4ne (14c-16e) $d\pi$ - $p\pi$ π -conjugation.

The aromaticity of **3** was further confirmed by the isomerization stabilization energy (ISE) values (39) and anisotropy of the induced current density (AICD) analysis (40). As shown in Fig. 4, the calculated ISE results are comparable to the values reported for other metalla-aromatics (Fig. 4B) (25–28, 30–32, 34). The clockwise ring current density of **3'** on the AICD isosurface indicates that **3** is aromatic (Fig. 4C). All calculation results are in good agreement with the experimental results, indicating that tetracyclic complex **3** is aromatic. Therefore, complex **3** represents the first example of a transition metal shared by four π aromatic units simultaneously.

UV-vis-NIR absorption spectra and photothermal properties

With such a unique aromatic framework, will these tetracyclic complexes have novel properties? To address this question, we examined the UV-visible (UV-vis) absorption spectra of these unique π -conjugated complexes. As shown in Fig. 5A, metal-bridgehead tetracyclic complexes **3a** to **3e** showed remarkably broad absorption from the UV to the visible region and up to 850 nm (NIR region), probably due to the extended conjugation framework in metalla-aromatic **3**. For instance, the absorption maximum of tetracyclic complex **3a** ($\lambda_{\text{max}} = 747$ nm) was red shifted by 119 nm compared with that of tricyclic complex **2** ($\lambda_{\text{max}} = 628$ nm). Time-dependent DFT calculations at the B3LYP/6-31G(d) level were used to describe the absorption spectrum of **3a**. The absorption bands at 747 and 648 nm can be assigned to the HOMO→LUMO and HOMO→LUMO + 1 electronic transitions (table S1), respectively. The NIR absorption spectra of these metal-bridgehead tetracyclic systems indicated their excellent photothermal properties (Fig. 5B). For example, the solution containing complex **3a** (1.00 mg/ml) exhibits a significant temperature increase from 29° to 79°C within 5 min under NIR laser (808 nm, 1 W/cm²) irradiation,

while the pure solvent shows a negligible temperature change under similar conditions. These results suggest their potential applications in photoelectric materials or biomedicine (32).

CONCLUSION

In summary, metalla-click reactions between azides and metal-carbon triple bonds have been used as a new annulation strategy, affording an efficient, precise synthesis of an extraordinary polycyclic species consisting of four fused five-membered aromatic metallacycles sharing with a bridgehead metal center. The unusual topology represents an unprecedented case in a fused-ring aromatic system with a congested center, which breaks through the previous limitation of up to three π -aromatic rings. This approach not only extends the accessible range of classical click reactions but also offers insight into previously inaccessible aromatic skeletons with congested centers, which would ultimately inspire further investigation of discovering challenging and complex aromatic molecular architectures.

MATERIALS AND METHODS

Details of the synthesis and characterization of complexes **2'** and **3b** to **3e** can be found in the Supplementary Materials. The synthetic procedures for **2** and **3a** are described below. The detailed crystal structures of complexes **2'** and **3c**, as well as all of the HRMS and NMR spectra discussed in this article can be found in the Supplementary Materials.

Synthesis of complex **2**

A mixture of compound **1** (200 mg, 0.15 mmol) and K_2CO_3 (103 mg, 0.75 mmol) in 10 ml of *N,N*-dimethylformamide was stirred at 40°C for 2 days to give a green solution. The solution was evaporated to dryness under vacuum. Then, the residue was extracted with dichloromethane (5 ml \times 3) and filtered. The extractant was concentrated to approximately 3 ml. Subsequent addition of diethyl ether (20 ml) to the extractant gave a green precipitate, which was collected by filtration, washed with diethyl ether (10 ml \times 2), and dried under vacuum. Yield: 138 mg, 74%. 1H NMR plus 1H - ^{13}C HSQC (600.1 MHz, CD_2Cl_2): 8.75 (s, 1H, H5), 7.63 (s, 1H, H3, confirmed by 1H - ^{13}C HSQC), 7.08 (s, 1H, H8, confirmed by 1H - ^{13}C HSQC), 3.82 (s, 3H, $COOCH_3$), and 7.85 to 7.00 ppm (50H, other aromatic protons). ^{31}P NMR (242.9 MHz, CD_2Cl_2): δ = 6.82 (s, $OsPPh_3$), 5.21 ppm (s, $CPPH_3$). ^{13}C NMR plus DEPT-135, 1H - ^{13}C HSQC, and 1H - ^{13}C HMBC (150.9 MHz, CD_2Cl_2): δ = 337.2 (td, J_{PC} = 16.3 Hz, J_{PC} = 14.4 Hz, C1), 231.1 (t, J_{PC} = 6.1 Hz, C7), 193.7 (s, C9), 165.1 (s, $COOCH_3$), 162.5 (s, C5), 159.4 (dt, J_{PC} = 26.4 Hz, J_{PC} = 3.1 Hz, C4), 141.4 (d, J_{PC} = 18.4 Hz, C3), 138.3 (s, C6), 116.2 (s, C8), 115.0 (d, J_{PC} = 99.1 Hz, C2), 51.4 (s, $COOCH_3$), and 137.4 to 127.0 ppm (other aromatic carbons). HRMS [electrospray ionization (ESI)]: m/z calcd for $[C_{71}H_{56}O_3OsP_3]^+$, 1241.3059; found, 1241.3037. Elemental analysis calcd (%) for $C_{95}H_{76}BO_3OsP_3$: C 66.84, H 4.42; found: C 66.48, H 4.32.

Synthesis of complex **3a**

Benzyl azide (56 μ l, 0.45 mmol) was added to a solution of **2** (190 mg, 0.15 mmol) in 10 ml of dichloromethane. The reaction mixture was stirred for 6 hours to give a green solution. Then, the mixture was concentrated to approximately 2 ml under vacuum and washed with diethyl ether (3 \times 30 ml) to afford a green solid. Yield: 193 mg,

92%. 1H NMR plus 1H - ^{13}C HSQC (500.2 MHz, $CDCl_3$): δ = 8.11 (s, 1H, H5), 7.97 (s, 1H, H8), 7.48 (s, 1H, H3, confirmed by 1H - ^{13}C HSQC), 5.21 (s, 2H, H10), 3.87 (s, 3H, $COOCH_3$), and 7.78 to 6.81 ppm (55H, other aromatic protons). ^{31}P NMR (202.5 MHz, $CDCl_3$): δ = 11.41 (s, $CPPH_3$) and -21.46 ppm (s, $OsPPh_3$). ^{13}C NMR plus DEPT-135, 1H - ^{13}C HSQC, and 1H - ^{13}C HMBC (125.8 MHz, $CDCl_3$): δ = 234.6 (t, J_{PC} = 6.9 Hz, C1), 226.5 (t, J_{PC} = 8.4 Hz, C7), 191.7 (s, C9), 166.5 (d, J_{PC} = 26.0 Hz, C4), 165.7 (s, C5), 164.3 (s, $COOCH_3$), 164.2 (d, J_{PC} = 14.8 Hz, C3), 137.6 (s, C6), 120.9 (s, C8), 114.1 (d, J_{PC} = 86.8 Hz, C2), 61.5 (s, C10), 51.3 (s, $COOCH_3$), and 137.4 to 120.7 ppm (other aromatic carbons). HRMS (ESI): m/z calcd for $[C_{78}H_{63}N_3O_3OsP_3]^+$, 1374.3700; found, 1374.3723. Elemental analysis calcd (%) for $C_{78}H_{63}ClN_3O_3OsP_3$: C 66.49, H 4.51, N 2.98; found: C 66.71, H 4.90, N 2.70.

SUPPLEMENTARY MATERIALS

Supplementary material for this article is available at <http://advances.sciencemag.org/cgi/content/full/6/3/eaay2535/DC1>

Supplementary Information Text

Synthetic Procedures

Cartesian coordinate-optimized structures for calculation

Fig. S1. $^{31}P\{^1H\}$ NMR spectrum of the starting material, complex **2**, and the in situ ^{31}P NMR spectra for the reaction of **2** with azide at room temperature.

Fig. S2. ACID isosurface of the model **3'** from the contribution of eight π -MOs.

Fig. S3. Positive-ion ESI-MS spectrum of $[2]^+ [C_{71}H_{56}O_3OsP_3]^+$ measured in dichloromethane.

Fig. S4. Positive-ion ESI-MS spectrum of $[2']^+ [C_{71}H_{56}O_3OsP_3]^+$ measured in dichloromethane.

Fig. S5. Positive-ion ESI-MS spectrum of $[3a]^+ [C_{78}H_{63}N_3O_3OsP_3]^+$ measured in dichloromethane.

Fig. S6. Positive-ion ESI-MS spectrum of $[3b]^+ [C_{77}H_{61}N_3O_3OsP_3]^+$ measured in dichloromethane.

Fig. S7. Positive-ion ESI-MS spectrum of $[3c]^+ [C_{78}H_{63}N_3O_4OsP_3]^+$ measured in dichloromethane.

Fig. S8. Positive-ion ESI-MS spectrum of $[3d]^+ [C_{78}H_{60}F_3N_3O_3OsP_3]^+$ measured in dichloromethane.

Fig. S9. Positive-ion ESI-MS spectrum of $[3e]^+ [C_{76}H_{67}N_3O_5OsP_3]^+$ measured in dichloromethane.

Fig. S10. 1H NMR (600.1 MHz, CD_2Cl_2) spectrum (inset: partial 1H - ^{13}C HSQC spectrum) for complex **2**.

Fig. S11. $^{31}P\{^1H\}$ NMR (242.9 MHz, CD_2Cl_2) spectrum for complex **2**.

Fig. S12. $^{13}C\{^1H\}$ NMR (150.9 MHz, CD_2Cl_2) spectrum for complex **2**.

Fig. S13. Two-dimensional 1H - ^{13}C HSQC spectrum for complex **2** in CD_2Cl_2 .

Fig. S14. Two-dimensional 1H - ^{13}C HMBC spectrum for complex **2** in CD_2Cl_2 .

Fig. S15. DEPT-135 spectrum (150.9 MHz, CD_2Cl_2) of complex **2**.

Fig. S16. 1H NMR (600.1 MHz, CD_2Cl_2) spectrum (inset: partial 1H - ^{13}C HSQC spectrum) for complex **2'**.

Fig. S17. $^{31}P\{^1H\}$ NMR (242.9 MHz, CD_2Cl_2) spectrum for complex **2'**.

Fig. S18. $^{13}C\{^1H\}$ NMR (150.9 MHz, CD_2Cl_2) spectrum for complex **2'**.

Fig. S19. Two-dimensional 1H - ^{13}C HSQC spectrum for complex **2'** in CD_2Cl_2 .

Fig. S20. Two-dimensional 1H - ^{13}C HMBC spectrum for complex **2'** in CD_2Cl_2 .

Fig. S21. DEPT-135 spectrum (150.9 MHz, CD_2Cl_2) of complex **2'**.

Fig. S22. $^{11}B\{^1H\}$ NMR (192.5 MHz, CD_2Cl_2) spectrum for complex **2'**.

Fig. S23. 1H NMR (500.2 MHz, $CDCl_3$) spectrum (inset: partial 1H - ^{13}C HSQC spectrum) for complex **3a**.

Fig. S24. $^{31}P\{^1H\}$ NMR (202.5 MHz, $CDCl_3$) spectrum for complex **3a**.

Fig. S25. $^{13}C\{^1H\}$ NMR (125.8 MHz, $CDCl_3$) spectrum for complex **3a**.

Fig. S26. Two-dimensional 1H - ^{13}C HSQC spectrum for complex **3a** in $CDCl_3$.

Fig. S27. Two-dimensional 1H - ^{13}C HMBC spectrum for complex **3a** in $CDCl_3$.

Fig. S28. DEPT-135 spectrum (125.8 MHz, $CDCl_3$) of complex **3a**.

Fig. S29. 1H NMR (500.2 MHz, CD_2Cl_2) spectrum (inset: partial 1H - ^{13}C HSQC spectrum) for complex **3b**.

Fig. S30. $^{31}P\{^1H\}$ NMR (202.5 MHz, CD_2Cl_2) spectrum for complex **3b**.

Fig. S31. $^{13}C\{^1H\}$ NMR (125.8 MHz, CD_2Cl_2) spectrum for complex **3b**.

Fig. S32. Two-dimensional 1H - ^{13}C HSQC spectrum for complex **3b** in CD_2Cl_2 .

Fig. S33. Two-dimensional 1H - ^{13}C HMBC spectrum for complex **3b** in CD_2Cl_2 .

Fig. S34. DEPT-135 spectrum (125.8 MHz, CD_2Cl_2) of complex **3b**.

Fig. S35. 1H NMR (500.2 MHz, CD_2Cl_2) spectrum (inset: partial 1H - ^{13}C HSQC spectrum) for complex **3c**.

Fig. S36. $^{31}P\{^1H\}$ NMR (202.5 MHz, CD_2Cl_2) spectrum for complex **3c**.

Fig. S37. $^{13}C\{^1H\}$ NMR (125.8 MHz, CD_2Cl_2) spectrum for complex **3c**.

Fig. S38. Two-dimensional 1H - ^{13}C HSQC spectrum for complex **3c** in CD_2Cl_2 .

Fig. S39. Two-dimensional 1H - ^{13}C HMBC spectrum for complex **3c** in CD_2Cl_2 .

Fig. S40. DEPT-135 spectrum (125.8 MHz) of complex **3c**.

Fig. S41. 1H NMR (500.2 MHz, CD_2Cl_2) spectrum (inset: partial 1H - ^{13}C HSQC spectrum) for complex **3d**.

Fig. S42. $^{31}\text{P}\{^1\text{H}\}$ NMR (202.5 MHz, CD_2Cl_2) spectrum for complex **3d**.
 Fig. S43. $^{13}\text{C}\{^1\text{H}\}$ NMR (125.8 MHz, CD_2Cl_2) spectrum for complex **3d**.
 Fig. S44. $^{19}\text{F}\{^1\text{H}\}$ NMR (376.4 MHz, CD_2Cl_2) spectrum for complex **3d**.
 Fig. S45. Two-dimensional ^1H - ^{13}C HSQC spectrum for complex **3d** in CD_2Cl_2 .
 Fig. S46. Two-dimensional ^1H - ^{13}C HMQC spectrum for complex **3d** in CD_2Cl_2 .
 Fig. S47. DEPT-135 spectrum (125.8 MHz, CD_2Cl_2) of complex **3d**.
 Fig. S48. ^1H NMR (500.2 MHz, CD_2Cl_2) spectrum (inset: partial ^1H - ^{13}C HSQC spectrum) for complex **3e**.
 Fig. S49. $^{31}\text{P}\{^1\text{H}\}$ NMR (202.5 MHz, CD_2Cl_2) spectrum for complex **3e**.
 Fig. S50. $^{13}\text{C}\{^1\text{H}\}$ NMR (125.8 MHz, CD_2Cl_2) spectrum for complex **3e**.
 Fig. S51. Two-dimensional ^1H - ^{13}C HSQC spectrum for complex **3e** in CD_2Cl_2 .
 Fig. S52. Two-dimensional ^1H - ^{13}C HMQC spectrum for complex **3e** in CD_2Cl_2 .
 Fig. S53. DEPT-135 spectrum (125.8 MHz, CD_2Cl_2) of complex **3e**.
 Table S1. Calculated absorption spectral data for **3a**.
 Table S2. Comparison of bond lengths in **3c** from the B3LYP functional and experimental data.
 Data file S1. CIF files for complexes **2'**.
 Data file S2. CIF files for complexes **3c**.
 References (41–56)

REFERENCES AND NOTES

- Z. Sun, Z. Zeng, J. Wu, Zethrenes, extended *p*-quinodimethanes, and periacenes with a singlet biradical ground state. *Acc. Chem. Res.* **47**, 2582–2591 (2014).
- M. Ball, Y. Zhong, Y. Wu, C. Schenck, F. Ng, M. Steigerwald, S. Xiao, C. Nuckolls, Contorted polycyclic aromatics. *Acc. Chem. Res.* **48**, 267–276 (2015).
- A. Narita, X.-Y. Wang, X. Feng, K. Müllen, New advances in nanographene chemistry. *Chem. Soc. Rev.* **44**, 6616–6643 (2015).
- M. Rickhaus, M. Mayor, M. Juriček, Strain-induced helical chirality in polyaromatic systems. *Chem. Soc. Rev.* **45**, 1542–1556 (2016).
- C. K. Frederickson, B. D. Rose, M. M. Haley, Explorations of the indenofluorenes and expanded quinoidal analogues. *Acc. Chem. Res.* **50**, 977–987 (2017).
- S. H. Pun, Q. Miao, Toward negatively curved carbons. *Acc. Chem. Res.* **51**, 1630–1642 (2018).
- U. H. F. Bunz, J. U. Engelhart, B. D. Lindner, M. Schaffroth, Large N-heteroacenes: New tricks for very old dogs? *Angew. Chem. Int. Ed.* **52**, 3810–3821 (2013).
- W. Jiang, Y. Li, Z. Wang, Heteroarenes as high performance organic semiconductors. *Chem. Soc. Rev.* **42**, 6113–6127 (2013).
- J. C. Buttrick, B. T. King, Kekulenes, cycloarenes, and heterocycloarenes: Addressing electronic structure and aromaticity through experiments and calculations. *Chem. Soc. Rev.* **46**, 7–20 (2017).
- M. Stepień, E. Gońka, M. Żyła, N. Sprutta, Heterocyclic nanographenes and other polycyclic heteroaromatic compounds: Synthetic routes, properties, and applications. *Chem. Rev.* **117**, 3479–3716 (2017).
- H. Tsuji, E. Nakamura, Design and functions of semiconducting fused polycyclic furans for optoelectronic applications. *Acc. Chem. Res.* **50**, 396–406 (2017).
- Z. Cai, M. A. Awais, N. Zhang, L. Yu, Exploration of syntheses and functions of higher ladder-type π -conjugated heteroacenes. *Chem* **4**, 2538–2570 (2018).
- L. J. Wright, *Metallabenzenes: An Expert View* (John Wiley & Sons Ltd., 2017).
- J. Chen, G. Jia, Recent development in the chemistry of transition metal-containing metallabenzenes and metallabenzynes. *Coord. Chem. Rev.* **257**, 2491–2521 (2013).
- B. J. Frogley, L. J. Wright, Fused-ring metallabenzenes. *Coord. Chem. Rev.* **270–271**, 151–166 (2014).
- I. Fernández, G. Frenking, G. Merino, Aromaticity of metallabenzenes and related compounds. *Chem. Soc. Rev.* **44**, 6452–6463 (2015).
- Y. Zhang, J. Wei, Y. Chi, X. Zhang, W.-X. Zhang, Z. Xi, Spiro metalla-aromatics of Pd, Pt, and Rh: Synthesis and characterization. *J. Am. Chem. Soc.* **139**, 5039–5042 (2017).
- J. Wei, W.-X. Zhang, Z. Xi, The aromatic dianion metalloles. *Chem. Sci.* **9**, 560–568 (2018).
- C. Zhu, H. Xia, Carbolong chemistry: A story of carbon chain ligands and transition metals. *Acc. Chem. Res.* **51**, 1691–1700 (2018).
- Y. Zhang, J. Wei, M. Zhu, Y. Chi, W.-X. Zhang, S. Ye, Z. Xi, Tetralithio metalla-aromatics with two independent perpendicular dithio aromatic rings spiro-fused by one manganese atom. *Angew. Chem. Int. Ed.* **58**, 9625–9631 (2019).
- M. Meldal, C. W. Tornøe, Cu-catalyzed azide-alkyne cycloaddition. *Chem. Rev.* **108**, 2952–3015 (2008).
- J. E. Hein, V. V. Fokin, Copper-catalyzed azide-alkynycycloaddition (CuAAC) and beyond: New reactivity of copper(I) acetylides. *Chem. Soc. Rev.* **39**, 1302–1315 (2010).
- D. H. Ess, G. O. Jones, K. N. Houk, Transition states of strain-promoted metal-free click chemistry: 1,3-dipolar cycloadditions of phenyl azide and cyclooctynes. *Org. Lett.* **10**, 1633–1636 (2008).
- S. Xie, S. A. Lopez, O. Ramström, M. Yan, K. N. Houk, 1,3-Dipolar cycloaddition reactivities of perfluorinated aryl azides with enamines and strained dipolarophiles. *J. Am. Chem. Soc.* **137**, 2958–2966 (2015).
- C. Zhu, S. Li, M. Luo, X. Zhou, Y. Niu, M. Lin, J. Zhu, Z. Cao, X. Lu, T. Wen, Z. Xie, P. v. Schleyer, H. Xia, Stabilization of anti-aromatic and strained five-membered rings with a transition metal. *Nat. Chem.* **5**, 698–703 (2013).
- C. Zhu, Y. Yang, J. Wu, M. Luo, J. Fan, J. Zhu, H. Xia, Five-membered cyclic metal carbyne: Synthesis of osmapentalynes by the reactions of osmapentalene with allene, alkyne, and alkene. *Angew. Chem. Int. Ed.* **54**, 7189–7192 (2015).
- Z. Lu, C. Zhu, Y. Cai, J. Zhu, Y. Hua, Z. Chen, J. Chen, H. Xia, Metallapentalenofurans and lactone-fused metallapentalynes. *Chem. A Eur. J.* **23**, 6426–6431 (2017).
- Q. Zhuo, J. Lin, Y. Hua, X. Zhou, Y. Shao, S. Chen, Z. Chen, J. Zhu, H. Zhang, H. Xia, Multiyne chains chelating osmium via three metal-carbon σ bonds. *Nat. Commun.* **8**, 1912 (2017).
- Q. Zhuo, H. Zhang, Y. Hua, H. Kang, X. Zhou, X. Lin, Z. Chen, J. Lin, K. Zhuo, H. Xia, Constraint of a ruthenium-carbon triple bond to a five-membered ring. *Sci. Adv.* **4**, eaat0336 (2018).
- C. Zhu, M. Luo, Q. Zhu, J. Zhu, P. v. Schleyer, J. I. Wu, X. Lu, H. Xia, Planar Möbius aromatic pentalenes incorporating 16 and 18 valence electron osmiums. *Nat. Commun.* **5**, 3265 (2014).
- C. Zhu, X. Zhou, H. Xing, K. An, J. Zhu, H. Xia, σ -Aromaticity in an unsaturated ring: Osmapentalene derivatives containing a metallacyclopentene unit. *Angew. Chem. Int. Ed.* **54**, 3102–3106 (2015).
- C. Zhu, C. Yang, Y. Wang, G. Lin, Y. Yang, X. Wang, J. Zhu, X. Chen, X. Lu, G. Liu, H. Xia, CCCC pentadentate chelates with planar Möbius aromaticity and unique properties. *Sci. Adv.* **2**, e1601031 (2016).
- M. Luo, L. Long, H. Zhang, Y. Yang, Y. Hua, G. Liu, Z. Lin, H. Xia, Reactions of isocyanides with metal carbyne complexes: Isolation and characterization of metallacyclopentimine intermediates. *J. Am. Chem. Soc.* **139**, 1822–1825 (2017).
- C. Zhu, J. Wu, S. Li, Y. Yang, J. Zhu, X. Lu, H. Xia, Synthesis and characterization of a metallacyclic framework with three fused five-membered rings. *Angew. Chem. Int. Ed.* **56**, 9067–9071 (2017).
- C. Zhu, J. Zhu, X. Zhou, Q. Zhu, Y. Yang, T. B. Wen, H. Xia, Isolation of an eleven-atom polydentate carbon-chain chelate obtained by cycloaddition of a cyclic osmium carbyne with an alkyne. *Angew. Chem. Int. Ed.* **57**, 3154–3157 (2018).
- C. M. Stegmair, W. Ullrich, W. Schütt, P. Kiprof, F. R. Kreißl, Synthese von 3H-1,2,3,4-triazametallo-komplexen durch addition von azidoameisensäure-methylester an die metall-kohlenstoff-dreifachbindung cyclopentadienyl-substituierter carbin-komplexe von molybdän und wolfram. *Chem. Ber.* **125**, 1571–1573 (1992).
- C. M. Stegmair, W. Schütt, W. Ullrich, P. Kiprof, J. Ostermeier, F. R. Kreißl, Darstellung und struktur von 1-metalla-2,3,4-triazolen des molybdäns und wolframs. *J. Organomet. Chem.* **447**, 251–257 (1993).
- Z. Chen, C. S. Wannere, C. Corminboeuf, R. Puchta, P. v. Schleyer, Nucleus-independent chemical shifts (NICS) as an aromaticity criterion. *Chem. Rev.* **105**, 3842–3888 (2005).
- C. S. Wannere, D. Moran, N. L. Allinger, B. A. Hess, L. J. Schaad, P. v. R. Schleyer, On the stability of large [4n]annulenes. *Org. Lett.* **5**, 2983–2986 (2003).
- D. Geuenich, K. Hess, F. Köhler, R. Herges, Anisotropy of the induced current density (ACID), a general method to quantify and visualize electronic delocalization. *Chem. Rev.* **105**, 3758–3772 (2005).
- K. D. Grimes, A. Gupte, C. C. Aldrich, Copper(II)-catalyzed conversion of aryl/heteroaryl boronic acids, boronates, and trifluoroborates into the corresponding azides: Substrate scope and limitations. *Synthesis* **2010**, 1441–1448 (2010).
- H. Kim, Y. J. Kang, E. S. Jeong, S. Kang, K. T. Kim, Glucose-responsive disassembly of polymersomes of sequence-specific boroxole-containing block copolymers under physiologically relevant conditions. *ACS Macro Lett.* **1**, 1194–1198 (2012).
- J. Sun, G. M. Stone, N. P. Balsara, R. N. Zuckermann, Structure–conductivity relationship for peptide-based PEO–mimetic polymer electrolytes. *Macromolecules* **45**, 5151–5156 (2012).
- P.-C. Li, Y.-C. Lin, M. Chen, S.-W. Kuo, Self-assembled structures from PEGylated polypeptide block copolymers synthesized using a combination of ATRP, ROP, and click chemistry. *Soft Matter* **9**, 11257–11269 (2013).
- O. V. Dolomanov, L. J. Bourhis, R. J. Gildea, J. A. K. Howard, H. Puschmann, OLEX2: A complete structure solution, refinement and analysis program. *J. Appl. Cryst.* **42**, 339–341 (2009).
- G. M. Sheldrick, SHELXT—Integrated space-group and crystal-structure determination. *Acta Crystallogr. A* **71**, 3–8 (2015).
- G. M. Sheldrick, Crystal structure refinement with SHELXL. *Acta Crystallogr. C* **71**, 3–8 (2015).
- M. J. Frisch, G. W. Trucks, H. B. Schlegel, G. E. Scuseria, M. A. Robb, J. R. Cheeseman, G. Scalmani, V. Barone, B. Mennucci, G. A. Petersson, H. Nakatsuji, M. Caricato, X. Li, H. P. Hratchian, A. F. Izmaylov, J. Bloino, G. Zheng, J. L. Sonnenberg, M. Hada, M. Ehara, K. Toyota, R. Fukuda, J. Hasegawa, M. Ishida, T. Nakajima, Y. Honda, O. Kitao, H. Nakai, T. Vreven, J. A. Montgomery Jr., J. E. Peralta, F. Ogliaro, M. Bearpark, J. J. Heyd, E. Brothers, K. N. Kudin, V. N. Staroverov, R. Kobayashi, J. Normand, K. Raghavachari, A. Rendell, J. C. Burant, S. S. Iyengar, J. Tomasi, M. Cossi, N. Rega, J. M. Millam, M. Klene, J. E. Knox,

- J. B. Cross, V. Bakken, C. Adamo, J. Jaramillo, R. Gomperts, R. E. Stratmann, O. Yazyev, A. J. Austin, R. Cammi, C. Pomelli, J. W. Ochterski, R. L. Martin, K. Morokuma, V. G. Zakrzewski, G. A. Voth, P. Salvador, J. J. Dannenberg, S. Dapprich, A. D. Daniels, O. Farkas, J. B. Foresman, J. V. Ortiz, J. Cioslowski, D. J. Fox, *Gaussian 09, Revision D.01* (Gaussian, Inc., 2009).
49. C. Lee, W. Yang, R. G. Parr, Development of the Colle-Salvetti correlation-energy formula into a functional of the electron density. *Phys. Rev. B* **37**, 785–789 (1988).
50. B. Miehlich, A. Savin, H. Stoll, H. Preuss, Results obtained with the correlation energy density functionals of Becke and Lee, Yang and Parr. *Chem. Phys. Lett.* **157**, 200–206 (1989).
51. A. D. Becke, Density-functional thermochemistry. III. The role of exact exchange. *J. Chem. Phys.* **98**, 5648–5652 (1993).
52. P. J. Hay, W. R. Wadt, Ab initio effective core potentials for molecular calculations. Potentials for K to Au including the outermost core orbitals. *J. Chem. Phys.* **82**, 299–310 (1985).
53. S. Huzinaga, *Gaussian Basis Sets for Molecular Calculations* (Elsevier, 1984).
54. R. Herges, D. Geuenich, Delocalization of electrons in molecules. *J. Phys. Chem. A* **105**, 3214–3220 (2001).
55. A. D. Becke, Density-functional exchange-energy approximation with correct asymptotic behavior. *Phys. Rev. A* **38**, 3098–3100 (1988).
56. G. Scalmani, M. J. Frisch, Continuous surface charge polarizable continuum models of solvation. I. General formalism. *J. Chem. Phys.* **132**, 114110 (2010).

Acknowledgments

Funding: This research was supported by the National Natural Science Foundation of China (nos. 21490573, 21572185, and U1705254). **Author contributions:** H.X. conceived the project. Z.L., Y.C., and K.Z. performed the experiments. Z.L. and Y.C. recorded all NMR data. Z.L. and Z.C. solved all x-ray structures. H.Z., Z.L., and H.X. analyzed the experimental data. H.Z. conceived the theoretical work. Q.Z. and Z.L. conducted the theoretical work. H.Z., Q.Z., Z.L., and J.Z. analyzed and interpreted the computational data. H.Z., Z.L., and H.X. drafted the paper. All of the authors discussed the results and contributed to the preparation of the final manuscript. **Competing interests:** The authors declare that they have no competing interests. **Data and materials availability:** All data needed to evaluate the conclusions in the paper are present in the paper and/or the Supplementary Materials. Additional data related to this paper may be requested from the authors. Crystal data of **2'** and **3c** are available from the Cambridge Crystallographic Data Centre under reference numbers CCDC-1818134 and 1818135 (www.ccdc.cam.ac.uk/data_request/cif).

Submitted 3 June 2019

Accepted 15 November 2019

Published 17 January 2020

10.1126/sciadv.aay2535

Citation: Z. Lu, Q. Zhu, Y. Cai, Z. Chen, K. Zhuo, J. Zhu, H. Zhang, H. Xia, Access to tetracyclic aromatics with bridgehead metals by metalla-click reaction. *Sci. Adv.* **6**, eaay2535 (2020).

Access to tetracyclic aromatics with bridgehead metals via metalla-click reactions

Zhengyu Lu, Qin Zhu, Yuanting Cai, Zhixin Chen, Kaiyue Zhuo, Jun Zhu, Hong Zhang and Haiping Xia

Sci Adv **6** (3), eaay2535.

DOI: 10.1126/sciadv.aay2535

ARTICLE TOOLS

<http://advances.sciencemag.org/content/6/3/eaay2535>

SUPPLEMENTARY MATERIALS

<http://advances.sciencemag.org/content/suppl/2020/01/13/6.3.eaay2535.DC1>

REFERENCES

This article cites 53 articles, 2 of which you can access for free
<http://advances.sciencemag.org/content/6/3/eaay2535#BIBL>

PERMISSIONS

<http://www.sciencemag.org/help/reprints-and-permissions>

Use of this article is subject to the [Terms of Service](#)

Science Advances (ISSN 2375-2548) is published by the American Association for the Advancement of Science, 1200 New York Avenue NW, Washington, DC 20005. The title *Science Advances* is a registered trademark of AAAS.

Copyright © 2020 The Authors, some rights reserved; exclusive licensee American Association for the Advancement of Science. No claim to original U.S. Government Works. Distributed under a Creative Commons Attribution NonCommercial License 4.0 (CC BY-NC).